Nonlinear Dyn (2021) 104:3937–3954
https://doi.org/10.1007/s11071-021-06502-3

ORIGINAL PAPER

Application of the improved NOFRFs weighted contribution rate based on KL divergence to rotor rub-impact

Haiying Liang · Huanhuan Lu · Kunpeng Feng · Yang Liu · Jintao Li · Lei Meng

Received: 6 January 2021 / Accepted: 27 April 2021 / Published online: 30 May 2021

Abstract As a common fault of the rotor system, the rub-impact between a rotor and a stator causes the rotor system to exhibit strong nonlinearities. Therefore, the vibration signals obtained from a rotor system with the rubbing fault contain weak high-order nonlinear components, which are difficult to be characterized by traditional linear methods. The nonlinear output frequency response functions (NOFRFs) are an effective approach for analyzing nonlinear systems in the frequency domain, which has been applied by many researchers in the fault diagnosis of nonlinear systems. In the present study, the concept of Kullback–Leibler (KL) divergence is introduced to NOFRFs to develop a novel method named the improved NOFRFs weighted contribution rate based on KL divergence (NWKL). And it is employed to detect the rotor system with a rub-impact fault. As a new index extracted by NWKL, the improved NOFRFs optimal weighted contribution rate based on KL divergence (*KLRm*) is proposed to evaluate the severity of rub-impact faults in rotor systems. The simulation and experimental results demonstrate high sensitivity and strong feature dynamic stability of the newly proposed index to rotor rub-impact. A new evaluation method named the feature dynamic stability analysis is proposed to explore the influence of the change in the friction coefficient and rub-impact stiffness on *KLRm*. The methods in this paper show the important significance and potential application values in the detection and evaluation of rotor rub-impact.

Keywords NOFRFs · Weighted contribution rate · Kullback–Leibler divergence · Rotor rub-impact · Fault diagnosis

H. Liang · H. Lu · K. Feng · Y. Liu (✉) · J. Li
School of Mechanical Engineering & Automation, Northeastern University, Shenyang 110819, China
e-mail: liuyang1982@mail.neu.edu.cn

Y. Liu
Key Laboratory of Vibration and Control of Aero-Propulsion System Ministry of Education, Northeastern University, Shenyang 110819, China

L. Meng
Shenyang Blower Works Group Co. Itd, Shenyang 110819, China

1 Introduction

As the core component of rotating machinery, the rotor system plays a vital role in the high-speed operation of equipment [1, 2]. As the requirements for the speed and efficiency of mechanical equipment are more demanding, the clearance between components is increasingly smaller, which renders rub-impact a more common fault for the rotor system [3]. The rubbing fault may affect the service life of the machine and even lead to catastrophic accidents. Therefore, it is of great engineering and practical

significance to research the methods of detecting and diagnosing the rubbing fault of the rotor system.

It is well known that the frequency response function (FRF) is a fundamental concept of linear systems and widely applied in engineering practice [4]. Some systems exhibit strong nonlinear characteristics, such as rotor systems with rub-impact faults [5–7]. An extension of the FRF theory to the nonlinear domain is known as the generalized frequency response functions (GFRFs), which were derived based on the Volterra series theory to describe the nonlinear characteristics of systems in the frequency domain. However, the GFRFs are rarely used to resolve complex engineering problems because it is tedious to calculate due to its multi-dimensional nature [8–10].

Lang and Billings proposed the concept of the nonlinear output frequency response functions (NOFRFs) based on the GFRFs to tackle this problem. The NOFRFs well explains the generation mechanism of nonlinear phenomena and provides a theoretical foundation for frequency domain analysis of nonlinear systems [11–14]. Therefore, it is extensively used to resolve some engineering problems such as structural health monitoring and fault diagnosis of complicated structures [15–19].

Peng [15, 16] employed the NOFRFs to detect cracks in beams and the position of nonlinear components in periodic structures. Bayma [17] designed a complete set of fatigue crack detection methods for beam structures by combining the NARX model with the NOFRFs. Based on the NOFRFs and the super-harmonic responses, Yao [18] proposed a detection strategy to locate the rub-impact fault in the rotor system. Cao [19] proposed a novel fault detection and diagnosis method for complicated nonlinear systems by combining the NOFRFs and evidence theory and employed this approach to diagnose the fault of the transmission system of a numerical control machine tool.

In order to improve the performance of the evaluated NOFRFs for nonlinear systems, scholars proposed associated indexes to reveal the system's dynamic characteristics [20–25]. Peng [20] proposed a simple NOFRFs-based index, *Fe*, to identify the damage of aluminum plates with holes and cracks. The experimental results demonstrated that the values of *Fe* of the inspected structure and those of a damage-free structure are quite distinct. Huang [21] introduced the information entropy to integrate the first four-order of NOFRFs and proposed a new index *Ne*, which is applied to detect the cumulative fatigue damage of fatigued plate specimens and used connecting rod parts. The obtained results revealed that *Ne* is more sensitive to different degrees of structural damage and can detect working time. Based on indexes of *Fe* and *Ne*, Liu [22–24] proposed an evaluated method named the NOFRFs weighted contribution rate and proposed an associated index, the second-order optimal weighted contribution rate denoted by *Rm*. The simulation and experimental results verified its sensitivity and superiority comparing to *Fe* and *Ne* in the fault diagnosis of rotor systems. Based on the concepts of KL divergence and NOFRFs, Mao [25] proposed the *NKL* detection index. And through the hammering frequency response experiment of the train wheelset, it was verified that *NKL* can effectively identify the fatigue damage and be proportional to the service time of the wheelset.

During the in-depth research of NOFRFs weighted contribution rate in Refs. [22–24], it is found that only the second-order weighted contribution rate is considered in this method but ignoring the influence of the system's nonlinearity on the other orders. Besides, as the severity of the fault increases, the values of this index *Rm* and its increments are relatively small and the sensitivity to faults is slightly lower. So it is necessary to propose a new index that can more fully characterize the system's nonlinearity and has greater sensitivity. Moreover, *Rm* is more easily affected by stiffness and friction coefficient. So this method can be improved, as well as the index of the second-order optimal weighted contribution rate.

In order to solve these problems, a new fault detection method named the improved NOFRFs weighted contribution rate based on KL divergence (NWKL) is proposed in this paper, which is applied to detect the rub-impact fault of the rotor system. And the associated index of the improved NOFRFs optimal weighted contribution rate based on KL divergence (*KLRm*) shows high sensitivity to rotor rub-impact both in simulation and experimental results. Compared to the previous method, the performance of the improved method is optimal. Finally, a novel evaluation method known as the feature dynamic stability analysis is proposed, which is applied to study the influence of the friction coefficients and rub-impact stiffness of the rubbing rotor system on the detection

method. And the simulation results verified the feature dynamic stability of the proposed method.

2 Related theory of the method of NWKL

2.1 The NOFRFs of nonlinear systems

The relationship between the input signal and the output signal of a nonlinear system in the time domain can be described as

$$y(t)=\sum_{n=1}^{N}\int_{-\infty}^{\infty}\cdots\int_{-\infty}^{\infty}h_n(\tau_1,\ldots,\tau_n)\prod_{i=1}^{n}u(t-\tau_i)\mathrm{d}\tau_i \tag{1}$$

where $u(t)$ and $y(t)$ are the input and output, respectively; $h_n(\tau_1,\cdots,\tau_n)$ is the nth Volterra kernel functions of the nonlinear system; N denotes the maximum order; τ is the time delay.

In the frequency domain, $U(j\omega_i)$ is the Fourier transform of $u(t)$. Then, the Fourier transform of $u^n(t)$ is expressed as

$$U_n(j\omega)=\frac{1/\sqrt{n}}{(2\pi)^{n-1}}\times\int_{\omega_1+\cdots+\omega_n=\omega}\prod_{i=1}^{n}U(j\omega_i)\mathrm{d}\sigma_{n\omega} \tag{2}$$

The expression for the output frequency response of the nonlinear system under general excitation is

$$Y(j\omega)=\sum_{n=1}^{N}Y_n(j\omega) \tag{3}$$

where $Y(j\omega)$ represents the Fourier transform of output signal; $Y_n(j\omega)$ denotes the nth-order output frequency response of the nonlinear system and is defined by

$$Y_n(j\omega)=\frac{1/\sqrt{n}}{(2\pi)^{n-1}}\times\int_{\omega_1+\cdots+\omega_n=\omega}H_n(j\omega_1,\cdots,j\omega_n)\prod_{i=1}^{n}U(j\omega_i)\mathrm{d}\sigma_{n\omega} \tag{4}$$

where $\int_{\omega_1+\cdots+\omega_n=\omega}H_n(j\omega_1,\cdots,j\omega_n)\prod_{i=1}^{n}U(j\omega_i)\mathrm{d}\sigma_{n\omega}$ denotes the integral of $H_n(j\omega_1,\cdots,j\omega_n)\prod_{i=1}^{n}U(j\omega_i)$ under the condition of $\omega_1+\cdots+\omega_n=\omega$ in the n-dimensional hyperplane. $H_n(j\omega_1,\cdots,j\omega_n)$ is the Fourier transform of $h_n(j\omega_1,\cdots,j\omega_n)$ and denotes the nth GFRFs of the nonlinear systems. Its expression is

$$H_n(j\omega_1,\ldots,j\omega_n)=\int_{-\infty}^{\infty}\cdots\int_{-\infty}^{\infty}h_n(\tau_1,\ldots,\tau_n)\times e^{-(\omega_1\tau_1+\cdots+\omega_n\tau_n)j}\mathrm{d}\tau_1\ldots\mathrm{d}\tau_n \tag{5}$$

Under the condition that $U_n(j\omega)\neq 0$, the NOFRFs are defined as

$$G_n(j\omega)=\frac{\int_{\omega_1+\cdots+\omega_n=\omega}H_n(j\omega_1,\cdots,j\omega_n)\prod_{i=1}^{n}U(j\omega_i)\mathrm{d}\sigma_{n\omega}}{\int_{\omega_1+\cdots+\omega_n=\omega}\prod_{i=1}^{n}U(j\omega_i)\mathrm{d}\sigma_{n\omega}} \tag{6}$$

Substituting Eq. (6) into Eq. (4), the output spectrum of the nth nonlinear system can be represented as

$$\begin{aligned}Y_n(j\omega)&=\frac{\int_{\omega_1+\cdots+\omega_n=\omega}H_n(j\omega_1,\cdots,j\omega_n)\prod_{i=1}^{n}U(j\omega_i)d\sigma_{n\omega}}{\int_{\omega_1+\cdots+\omega_n=\omega}\prod_{i=1}^{n}U(j\omega_i)d\sigma_{n\omega}}\\&\quad\times\frac{1/\sqrt{n}}{(2\pi)^{n-1}}\int_{\omega_1+\cdots+\omega_n=\omega}\prod_{i=1}^{n}U(j\omega_i)d\sigma_{n\omega}\\&=G_n(j\omega)U_n(j\omega)\end{aligned} \tag{7}$$

So the relationship between the input and output in the frequency domain can be rewritten by

$$Y(j\omega)=\sum_{n=1}^{N}Y_n(j\omega)=\sum_{n=1}^{N}G_n(j\omega)U_n(j\omega) \tag{8}$$

Considering that the first four-order output frequency response function of a nonlinear system can almost characterize its most nonlinear characteristics, only the first four orders of NOFRFs are calculated so as to simplify the calculation process and improve calculation efficiency [15].

Therefore, Eq. (8) can be further expressed as

$$Y(j\omega)=G_1(j\omega)U_1(j\omega)+G_3(j\omega)U_3(j\omega) \tag{9}$$

$$Y(j2\omega)=G_2(j2\omega)U_2(j2\omega)+G_4(j2\omega)U_4(j2\omega) \tag{10}$$

$$Y(j3\omega)=G_3(j3\omega)U_3(j3\omega) \tag{11}$$

$$Y(j4\omega)=G_4(j4\omega)U_4(j4\omega) \tag{12}$$

Through the analysis of Eqs. (9-12), it is found that when a nonlinear system is excited by two harmonic signals with different amplitudes but the same frequency, its first four orders of NOFRFs can be obtained by using the least square method.

When two different sinusoidal signals with different amplitudes but the same frequency are employed to excite a rotor system, the input spectra of the system are, respectively, expressed by $A_i^{(1)}(j\omega_F)$ and $A_i^{(2)}(j\omega_F)$, $i = 1, 2, 3, 4$. And the corresponding output spectra of the system $Y^{(1)}(j\omega_F)$ and $Y^{(2)}(j\omega_F)$ are expressed as

$$\begin{pmatrix} Y^{(1)}(j\omega_F) \\ Y^{(2)}(j\omega_F) \end{pmatrix} = \begin{pmatrix} A_1^{(1)}(j\omega_F) & A_3^{(1)}(j\omega_F) \\ A_1^{(2)}(j\omega_F) & A_3^{(2)}(j\omega_F) \end{pmatrix} \begin{pmatrix} G_1(j\omega_F) \\ G_3(j\omega_F) \end{pmatrix} \tag{13}$$

$G_1(j\omega_F)$ and $G_3(j\omega_F)$ can be calculated by

$$\begin{pmatrix} G_1(j\omega_F) \\ G_3(j\omega_F) \end{pmatrix} = \begin{pmatrix} A_1^{(1)}(j\omega_F) & A_3^{(1)}(j\omega_F) \\ A_1^{(2)}(j\omega_F) & A_3^{(2)}(j\omega_F) \end{pmatrix}^{-1} \begin{pmatrix} Y^{(1)}(j\omega_F) \\ Y^{(2)}(j\omega_F) \end{pmatrix} \tag{14}$$

Similarly, the other orders of NOFRFs can be obtained.

2.2 NWKL detection method

Based on the concepts of contribution rate and feature weighting, Liu [22–25] integrated them with the NOFRFs and proposed the method of NOFRFs weighted contribution rate, which is defined by

$$Rn(n)(\rho) = \frac{\int_{-\infty}^{+\infty} \left|\frac{G_n(j\omega)}{n^\rho}\right| \mathrm{d}\omega}{\sum_{i=1}^{N} \int_{-\infty}^{+\infty} \left|\frac{G_i(j\omega)}{i^\rho}\right| \mathrm{d}\omega}, \ 1 \le n \le N, \ \rho \in (-\infty, +\infty) \tag{15}$$

In the definition of the weighted contribution rate, the weighted coefficient n^ρ is applied to increase the contribution rate of high-order NOFRFs for the nonlinear system, which solves the problem of small values of high-order NOFRFs, as well as that of NOFRFs-based indexes.

In the fault diagnosis of the rotor system, it was found through deep research that the second-order weighted contribution rate can better indicate the severity of the failure. And its expression is

$$Rn2(\rho) = \frac{\int_{-\infty}^{+\infty} \left|\frac{G_2(j\omega)}{2^\rho}\right| \mathrm{d}\omega}{\sum_{i=1}^{N} \int_{-\infty}^{+\infty} \left|\frac{G_i(j\omega)}{i^\rho}\right| \mathrm{d}\omega} \tag{16}$$

For the curve of $Rn2(\rho)$ changing with ρ, the abscissa of the curve at the peak is named as the optimal fitness factor $\rho_{\max}$. And the corresponding weighted contribution rate at $\rho = \rho_{\max}$ is defined as the second-order optimal weighted contribution rate, the equation of which is as

$$Rm = \frac{\int_{-\infty}^{+\infty} \left|\frac{G_2(j\omega)}{2^{\rho_{\max}}}\right| \mathrm{d}\omega}{\sum_{i=1}^{N} \int_{-\infty}^{+\infty} \left|\frac{G_i(j\omega)}{i^{\rho_{\max}}}\right| \mathrm{d}\omega} \tag{17}$$

In the rotor experiment, the severity of the rub-impact fault can be distinguished by *Rm*. This NOFRFs-based index only considers the second-order weighted contribution rate while ignoring the influence of the other orders. So it does not fully reflect the degree of nonlinearities of the system. Moreover, it is found that as fault severity increases, the values of the *Rm* do not change significantly, and its sensitivity to faults is poor. And this index is easily affected by the friction coefficient and stiffness of the system.

Therefore, in order to construct a new index that can comprehensively reveal the nonlinearity of the system and better distinguish the severity of faults, as well as having better robustness, the concept of KL divergence is introduced to the NOFRFs weighted contribution rate method.

For a random variable, the KL divergence is used to distinguish its two continuous probability density distributions $f(x_i), i = 1, \cdots, N$ and $g(x_i), i = 1, \cdots, N$. And the definition of the KL divergence is defined by

$$D_{KL}(f \parallel g) = \sum_{i=1}^{N} f(x_i) \log \frac{f(x_i)}{g(x_i)} \tag{18}$$

For example, the distribution difference of second-order weighted contribution rate, for healthy rotor system and fault rotor system, can be represented by their KL divergence. The difference between two distributions is larger, the KL divergence will be larger. Therefore, to better measure the distribution difference between the healthy rotor system and the

detested-to-be rotor system with unknown fault conditions, an improved NOFRFs weighted contribution rate based on the KL divergence method (*KLRn*) is proposed, which is defined as

$$\begin{aligned} &KLRn(\rho) = KLRn1(\rho) + \cdots + KLRn\mathrm{N}(\rho) \\ &= \sum_{n=1}^{N} \left| Rn_h(n)(\rho) \log \frac{Rn_h(n)(\rho)}{Rn_t(n)(\rho)} \right|, 1 \le n \le N \end{aligned} \tag{19}$$

In Eq. (19), $Rn_h(n)(\rho)$ denotes the distribution of the nth-order weighted contribution rate changing with ρ of a healthy rotor system, while $Rn_t(n)(\rho)$ represents the distribution of the nth-order weighted contribution rate changing with ρ of the detested-to-be rotor system.

When the detested-to-be rotor system is a healthy rotor system, $Rn_t(n)(\rho)$ is almost equal to $Rn_h(n)(\rho)$ so $\log \frac{Rn_h(n)(\rho)}{Rn_t(n)(\rho)}$ is close to zero. Therefore, $KLRn(\rho)$ is approximately coincident with the x-axis.

If the rotor system to be tested is a faulty rotor system, for a specific $\rho = \rho_0$, the values of $KLRn(\rho_0)$ gradually increase with the fault of the rotor system becoming more serious, namely, $KLRn(\rho)$ is proportional to the system's nonlinearity. Therefore, this approach can comprehensively represent the nonlinear characteristics of a nonlinear system by fusing all orders of NOFRFs weighted contribution rate.

3 Simulation analysis

3.1 Finite element model of the rotor system

Jeffcott rotor system with a rub-impact fault between the rotor and the stator was adopted for simulation analysis. The shaft is divided into 11 shaft segments by 12 nodes. The specific parameters of segments are given in Table 1. Each shaft segment is modeled by the Timoshenko beam. The rub-impact rotor system is simplified by assuming that the rubbing between the rotor and the stator is a local elastic collision and the deformation is elastic deformation. The finite element model of the rub-impact rotor system studied in this paper is illustrated in Fig. 1. The shaft segments are denoted as the numbers, dots as the black marks. And the rub-impact occurs at the red mark (at node 9).

In order to ensure that the disk and the elastic rod meet the contact conditions and do not penetrate each other during the rubbing process, the Kuhn–Tucker condition of Coulomb friction is employed to detect the contact between the rotor and the stator. Contact constraint conditions are handled by the augmented Lagrangian method of friction. When a rub-impact fault occurs, the friction torque caused by it is ignored and only the normal and tangential rubbing forces, P_n and P_t, are considered. Their specific expressions are as follows.

$$\begin{aligned} P_n &= \begin{cases} 0, & r < \delta_0 \\ (r-\delta_0)k_c + \lambda_r^{(i+1)}, & r < \delta_0 \end{cases} \\ P_t &= f_c P_n \end{aligned} \tag{20}$$

where the specific expression of $\lambda_r^{(i+1)}$ is

$$\lambda_r^{(i+1)} = \begin{cases} \lambda_r^{(i)} + k_c \delta_r, & |\delta_r| \ge \varepsilon \\ \lambda_r^{(i)}, & |\delta_r| \ge \varepsilon \end{cases} \tag{21}$$

where ε is the specific penetration tolerance; $\delta_r = r - \delta_0$. In the iterative process, the contact stiffness of the contact unit is expanded through $\lambda_r^{(i+1)}$ until the penetration is less than the initial preset value.

The friction force of the rotor system can be expressed by

$$\begin{Bmatrix} F_{rubx} \\ F_{ruby} \end{Bmatrix} = -\mathrm{H}(\delta_r)\delta_r \frac{\delta_r k_c + \lambda_r^{(i+1)}}{r} \begin{pmatrix} 1 & -f_c \\ f_c & 1 \end{pmatrix} \begin{Bmatrix} x \\ y \end{Bmatrix} \tag{22}$$

where the Heaviside function is defined as

$$H(\delta_r) = \begin{cases} 1, \delta_r \ge 0 \\ 0, \delta_r < 0 \end{cases} \tag{23}$$

Table 1 Specific parameters of the segments

Segment no.	1	2	3	4	5	6	7	8	9	10	11
Diameter (mm)	10	10	10	10	10	70	10	10	10	10	10
Length (mm)	50	50	50	40	40	27	40	40	50	50	50

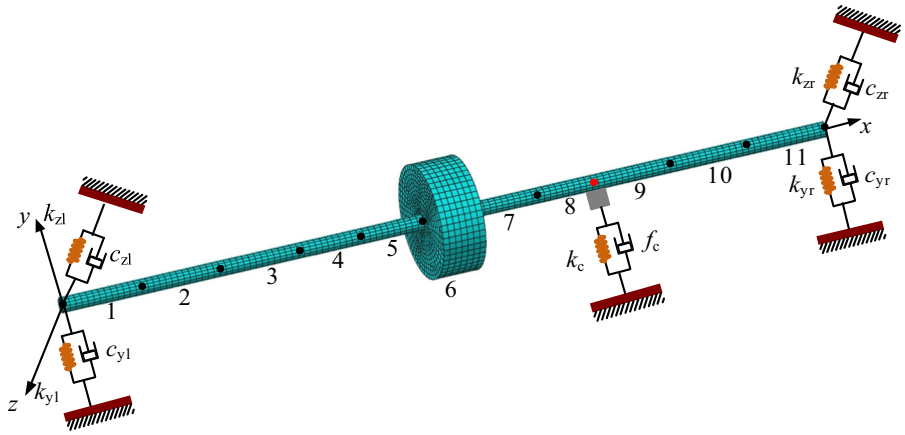

Fig. 1 Finite element model of the rub-impact rotor system

Therefore, the control equation of the rubbing rotor system is described as

$$\begin{cases} M\ddot{x}+(C+G)\dot{x}+Kx=F_{ex}+F_{rubx} \\ M\ddot{y}+(C+G)\dot{y}+Ky=F_{ey}+F_{ruby} \end{cases} \tag{24}$$

where **M**, **C**, **G**, and **K** represent mass matrix, damping matrix, gyro matrix, and stiffness matrix of the rotor system. And $\mathbf{F}_{ex}$ and $\mathbf{F}_{ey}$ are unbalanced force vectors of x and y directions.

The method of Newmark-β is applied to solve Eq. (24). The simulation information is given in Table 2. When the rub-impact gap is 120 μm, 80 μm, 40 μm, respectively, that is, the rotor system is, respectively, in the condition of normal, slight, moderate, and severe rub-impact fault, the dynamic responses of the rotor system at node 8 along the y-direction at a rotational speed of 1500 rpm are as shown in Fig. 2. Figure 2a shows the time responses and Fig. 2b shows the frequency responses. The x-axis represents frequency and the y-axis represents the clearance of the rub-impact. And the z-axis represents the amplitude of the frequency response.

It can be seen from Fig. 2a that when there is no rub-impact fault, that is, the rotor system is in normal working condition, the time domain waveform is a standard sine wave. As the rubbing clearance decreases from 120 μm to 40 μm, the standard sine wave increasingly deforms. The amplitude at the peak gradually increases and peak clipping at the trough is more sever. Figure 2b indicates that as the rub-impact clearance gradually decreases, the rub-impact fault renders super-harmonic components in the frequency domain response of the system. And the more serious the rub-impact fault degree is, the stronger nonlinearity of the system is so the larger the corresponding amplitude of the super-harmonic component is. Therefore, traditional linear methods are difficult to analyze characteristics of nonlinear systems.

Table 2 Simulation parameters of the finite element model

Parameters	Values
Material	45#steel
Young modulus of shaft Ef (G Pa)	210
Density (kg/m^3)	7850
Poisson's ratio v	0.3
Normal rub-impact stiffness ratio k	2×10^4
Friction coefficient c	0.1
Bearing stiffness (N/m)	2×10^6
Unbalance (kg·m)	$167.4 \times 10^{-6}/236.7 \times 10^{-6}$

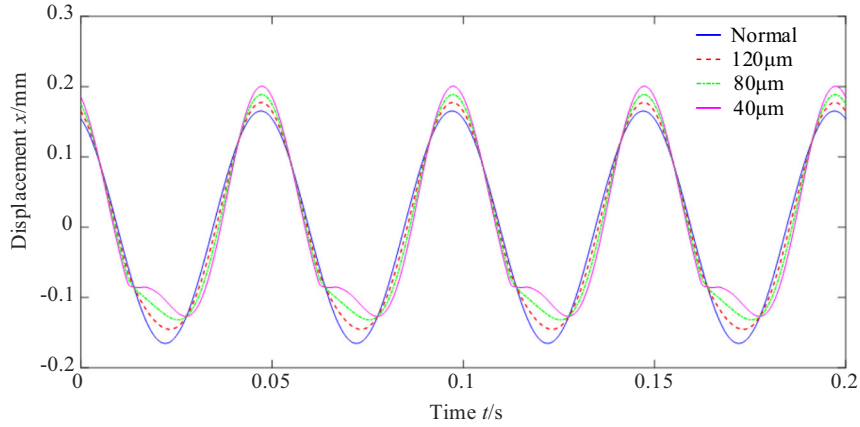

(a) Time domain response

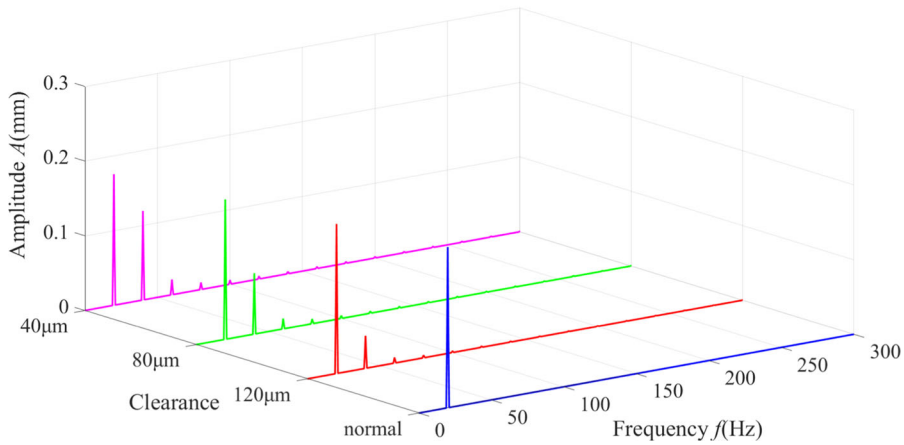

(b) Frequency domain response

Fig. 2 Dynamic responses with three different rub-impact conditions at 1500 r/min (**a-b**)

3.2 NWKL for the detection of rub-impact

Based on the related theory of NWKL and the dynamic response analysis of the rub-impact rotor system, this section employs the method of NWKL to analyze the simulation model of the rub-impact rotor system by assuming that system's nonlinearities can be fully represented when the maximum nonlinearity order $N = 4$. The working conditions of the simulation model are set to normal and the rub-impact fault with the rubbing clearance of 160 μm, 140 μm, 120 μm, 100 μm, 80 μm, 60 μm, 40 μm, and 20 μm, respectively. And vibration response signals at node 8 of the rotor system under different working conditions are obtained for subsequent analysis. The changing curves of the weighted contributed rate of the NOFRFs (Rn) with the adaptation factor ρ from -30 to 10 with a step of 1.0 under different rub-impact conditions are illustrated in Fig. 3.

It is obvious that changing trends of curves $Rn1$-$Rn4$ are quite distinct. It can be seen from Fig. 3a that curve $Rn1$ monotonically increases in the range of [0,1]. And for a certain ρ, the values of $Rn1$ under different conditions only slightly decrease as rub-impact faults are more sever. As shown in Fig. 3b, $Rn2$ increases from zero to the maximum value and then decreases to zero. And maximum values show an increasing trend along with the decrease of the rubbing clearance. However, the difference between the maximum value of $Rn2$ under the normal condition and the most sever rubbing fault is less than 0.05, which is a bit small. Figure 3c indicates that $Rn3$ follows

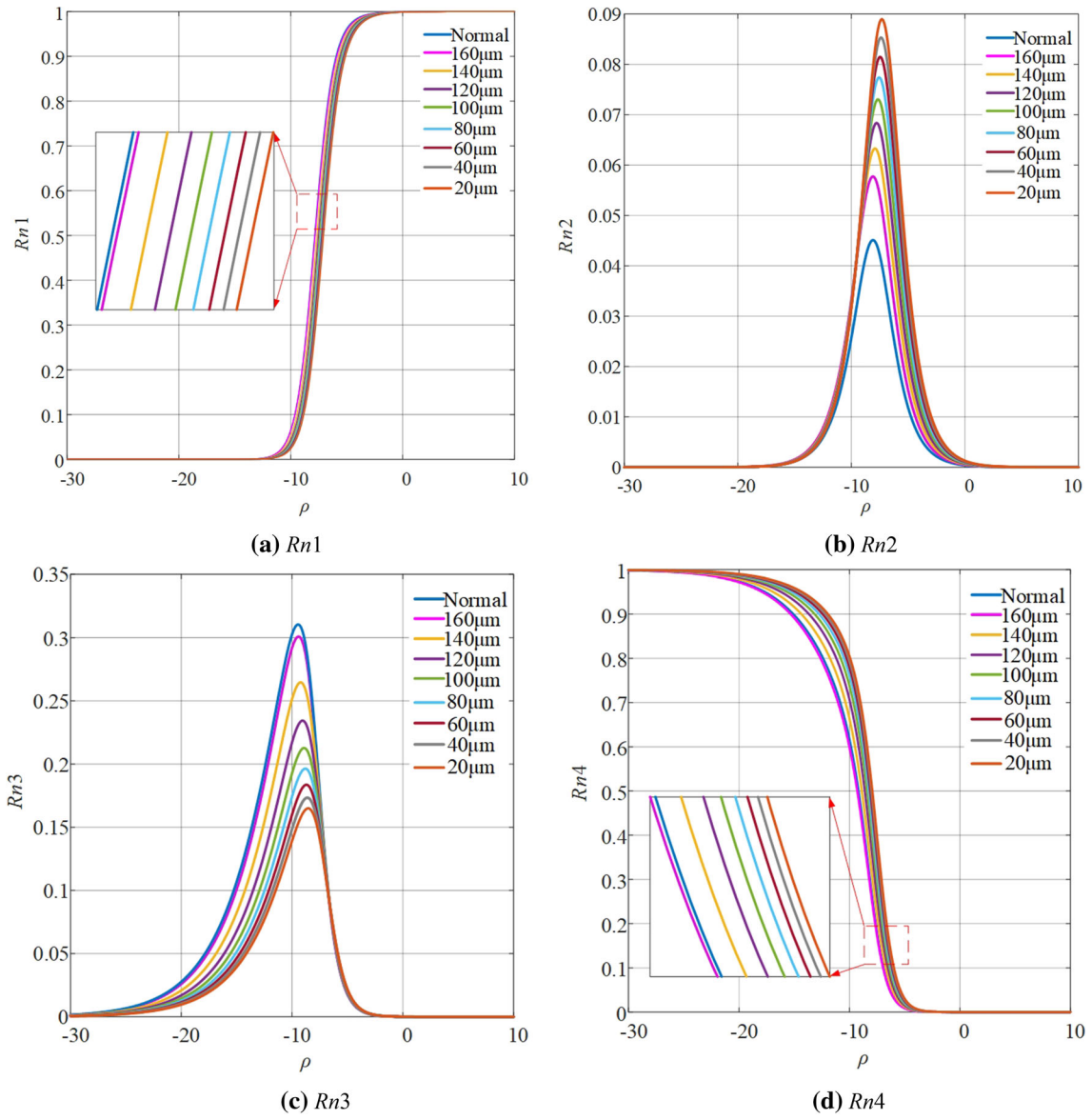

Fig. 3 Each order of *Rn* at different rub-impact conditions (**a-d**)

the same changing trend with *Rn*2 but maximum values show a decreasing trend with the increase of the fault severity. It is obvious from Fig. 3d that curve *Rn*4 monotonically decreases in the range of [0,1]. And for a certain ρ, the values of *Rn*4 only slightly increase with the severity of the rub-impact fault. But for the weakest rub-impact fault condition where the rub-impact gap is 160um, its value of *Rn*4 is less than that of the normal rotor system for a certain ρ, which is undesirable. In reference [25], the maximum value of *Rn*2 is defined as a new index *Rm* for the detection of rub-impact. On this basis, the authors conducted the following in-depth research.

The concept of KL divergence was introduced to the NOFRFs weighted contribution rate. After obtaining values of *Rn*1-*Rn*4, the corresponding values of each order of the improved NOFRFs weighted contributed rate based on KL divergence (respectively, denoted by *KLRn*1, *KLRn*2, *KLRn*3 and *KLRn*4) were further calculated through Eq. (19). And the changing curves of *KLRn*1-*KLRn*4 with the adaptation factor ρ from -30 to 10 with a step of 1.0

under different rub-impact conditions are illustrated as Fig. 4.

In Fig. 4, the changing trend of *KLRn*1, *KLRn*2, *KLRn*3, and *KLRn*4 increases from zero to the maximum value and then decreases to zero. And maximum values of each order of *KLRn* show an increasing trend as the severity of the rub-impact fault increases. Under the same condition, the values of *KLRn*1, *KLRn*2, *KLRn*3 and *KLRn*4 are different because each order *KLRn* has different sensitivity to nonlinearities for a nonlinear system.

In order to comprehensively consider the influence of the system's nonlinearity on *KLRn*1, *KLRn*2, *KLRn*3, and *KLRn*4, the value of *KLRn* is obtained by summing *KLRn*1-*KLRn*4. Figure 5 shows the

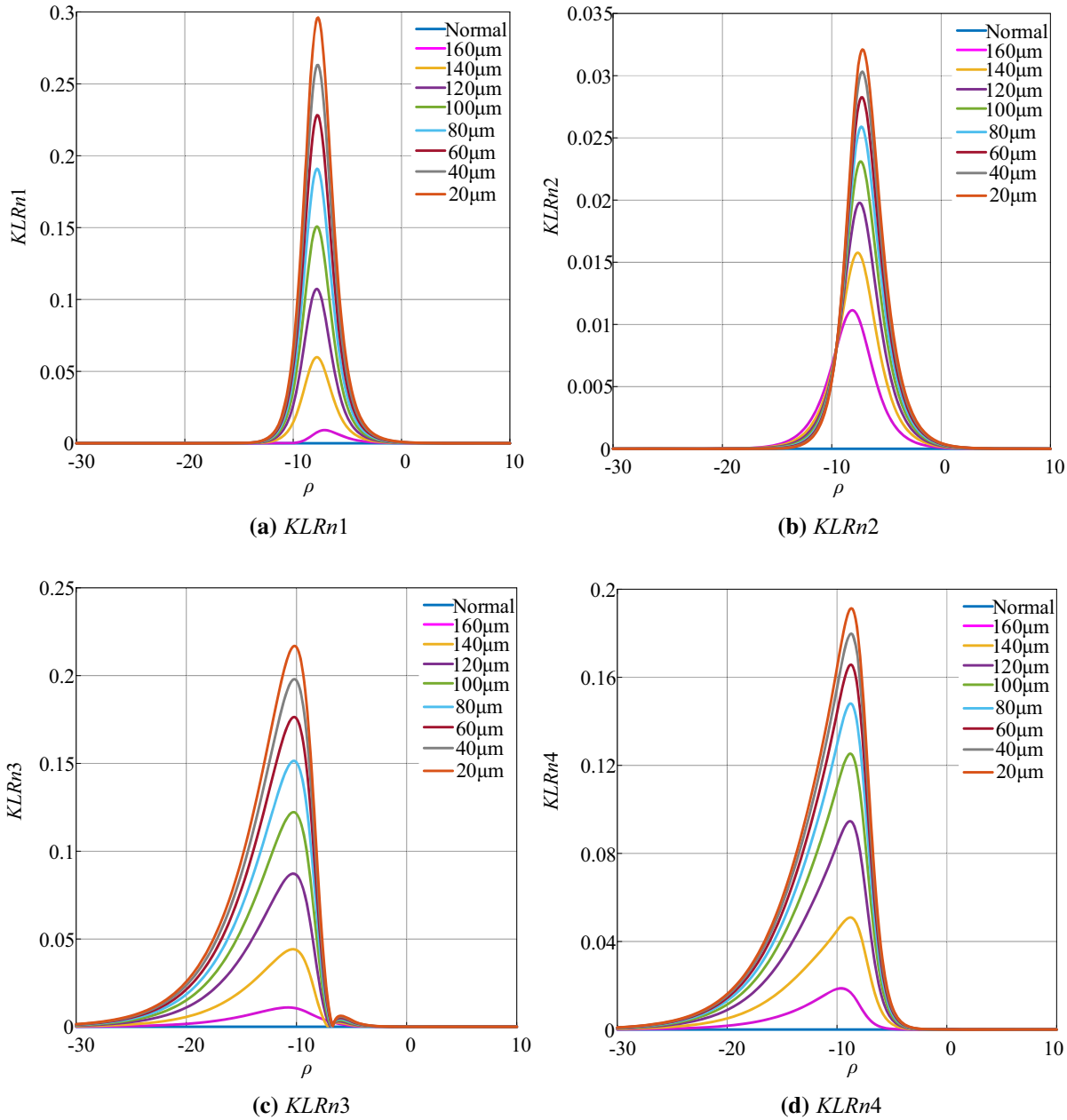

(a) *KLRn*1 **(b)** *KLRn*2

(c) *KLRn*3 **(d)** *KLRn*4

Fig. 4 Each order of *KLRn* at different rub-impact conditions (**a-d**)

changing curves of *KLRn* with the adaptation factor ρ under different rub-impact conditions.

In Fig. 5, the changing trend of *KLRn* increases from zero to the maximum value and then decreases to zero with the adaptation factor ρ changing from -30 to 10. And maximum values of *KLRn* under different conditions show an increasing trend starting from zero as the severity of the rub-impact fault increases.

3.3 The index of *KLRm*

Based on the analysis in Sect. 3.2, for the curve of $KLRn(\rho)$ changing with ρ, the abscissa of the curve at the peak is named as the optimal fitness factor $\rho_{\max}$. The corresponding maximum value of the curve at $\rho = \rho_{\max}$ is defined as a new indicator named improved NOFRFs optimal weighted contribution rate based on KL divergence (*KLRm*), the equation of which is as

$$KLRm = \max KLRn(\rho) \tag{25}$$

For showing the advantages of the proposed index, values of *KLRm* under different rub-impact conditions and their related optimal adaptation factor (ρ_{m2}) are compared with the values of *Rm* and their related optimal adaptation factor (ρ_{m1}), as given in Table 3. And comparison charts of *KLRm* with *Rm* at different rubbing gaps and their increments ($\triangle KLRm$ and $\triangle Rm$) are shown as Fig. 6.

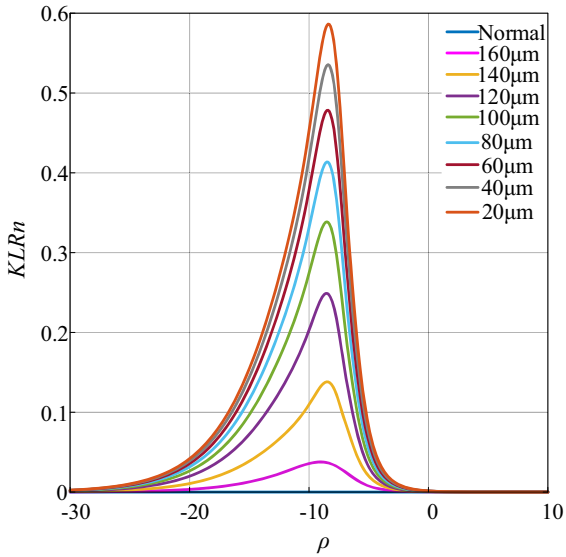

Fig. 5 Changing curve of *KLRn* under different rub-impact conditions

It is evident from Table 3 and Fig. 6 that values of *Rm* and *KLRm* both show an increasing trend as the severity of rubbing increases. And indexes *Rm* and *KLRm* can distinguish clearances of rub-impact so they can be employed to detect the rub-impact fault. However, values of *KLRm* start from zero and are larger than that of *Rm* under fault working conditions. Also, $\triangle KLRm$ is more obvious than $\triangle Rm$ under the same fault condition. Comparing optimal adaptation factors ρ_{m1} and ρ_{m2}, it is seen that the change of ρ_{m2} is smaller for different rubbing gaps. Therefore, the indicator *KLRm* is more sensitive and stable to the rub-impact fault of rotor systems.

3.4 Feature dynamic stability analysis

When the rub-impact occurs, friction conditions and rub-impact stiffness will significantly affect the dynamic responses of the rotor system [26]. Therefore, studying the influence of the friction coefficients and rub-impact stiffness on the proposed detection method is necessary. So authors proposed a new evaluation method named the feature dynamic stability analysis of the rubbing rotor system. This section will explore the influence of the change in the friction coefficient and rub-impact stiffness between the rotor and the stator on the values of *KLRm*.

In one case, the rub-impact stiffness is set to $k = 1 \times 10^4$ N/m and the friction coefficients are $c_1 = 0.1$, $c_2 = 0.2$ and $c_3 = 0.3$, respectively. The variation curves of *KLRn* and *Rn* with ρ under different conditions are shown in Figs.7, 8, 9. And the values of *KLRm* and *Rm* under different friction coefficients are shown in Fig. 10.

By comprehensive comparison of Figs.7, 8, 9, it can be seen that when the rub-impact stiffness is constant and the friction coefficient changes, the trend of the *KLRn* and *Rn* curves is almost unchanged but the maximum of the curve changes slightly. As shown in Fig. 10, in contrast, for the same type of rub-impact clearance, the change of the index *KLRm* is significantly smaller than that of *Rm* when the friction coefficient is different.

In another case, the friction coefficient is set to $c = 0.1$ and the rub-impact stiffness is $k_1 = 1 \times 10^4$ N/m, $k_2 = 2 \times 10^4$ N/m and $k_3 = 3 \times 10^4$ N/m, respectively. The values of *KLRm*

Table 3 Comparison of *KLRm* and *Rm*

Clearance (μm)	Normal	160	140	120	100	80	60	40	20
ρ_{m1}	− 8.1	− 8.1	− 7.9	− 7.8	− 7.7	− 7.6	− 7.5	− 7.4	− 7.3
Rm	0.04511	0.05775	0.06330	0.06837	0.07304	0.07739	0.08148	0.08534	0.08898
$\triangle Rm$	—	0.01264	0.00555	0.00507	0.00467	0.00435	0.00409	0.00386	0.00364
ρ_{m2}	—	− 8.9	− 8.5	− 8.5	− 8.5	− 8.5	− 8.4	− 8.4	− 8.4
KLRm	0	0.03779	0.13814	0.24898	0.33859	0.41368	0.47842	0.53553	0.58636
$\triangle KLRm$	—	0.03779	0.10035	0.11084	0.08961	0.07509	0.06474	0.05711	0.05083

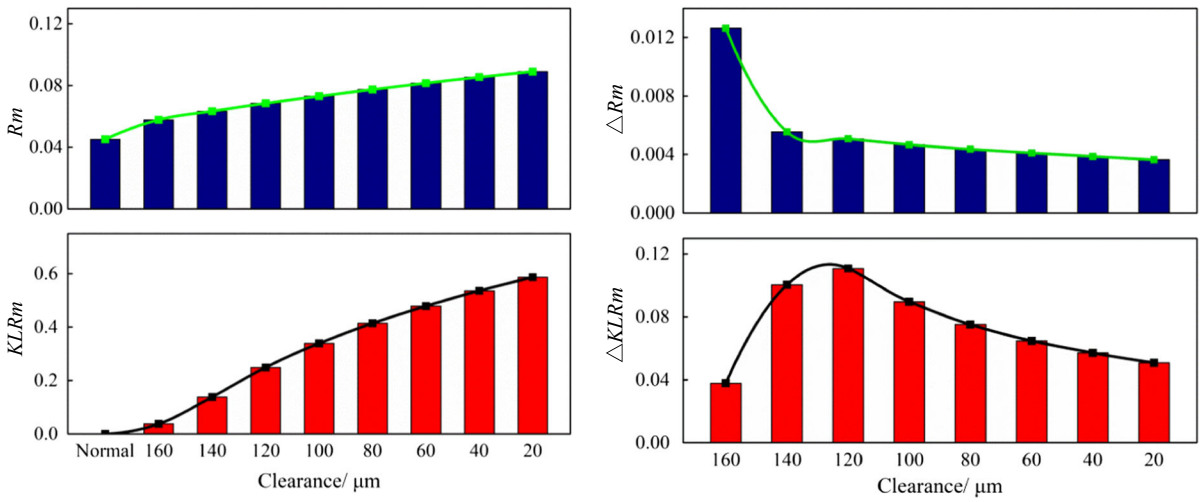

(a) Indices *KLRm* and *Rm* **(b)** The increment of indices *KLRm* and *Rm*

Fig. 6 Comparison charts of *KLRm* with *Rm* (**a**–**b**)

and *Rm* under different rub-impact stiffness are shown in Fig. 11.

Similarly, in Fig. 11, when the friction coefficient is constant and the rub-impact stiffness changes, the change of the index *KLRm* is also significantly smaller than that of *Rm* for the same type of rub-impact clearance.

Therefore, it is concluded that, compared to the method of NOFRFs weighted contribution rate, the improved NOFRFs weighted contribution rate method based on KL divergence has more robust feature dynamic stability.

3.5 Fault detection procedure

Based on the previous introduction, the method of improved NOFRFs weighted contribution rate based on the KL divergence for the rotor system's rub-impact fault detection procedure is as follows.

Step 1: Excite a healthy or a faulty rotor system twice using the signals with different amplitudes but the same frequency and collect the input and output signals.

Step 2: Calculate the first four orders of NOFRFs, $G_n(jw), n = 1, \cdots, 4,$ through Eq. (9)—Eq. (12) from the data obtained in Step 1.

Step 3: Calculate the distribution of the NOFRFs weighted contribution rate (*Rn*) with the change of ρ through Eq. (16).

Step 4: Calculate the distribution of the improved NOFRFs weighted contribution rate based on KL divergence (*KLRn*) with the change of ρ through Eq. (19).

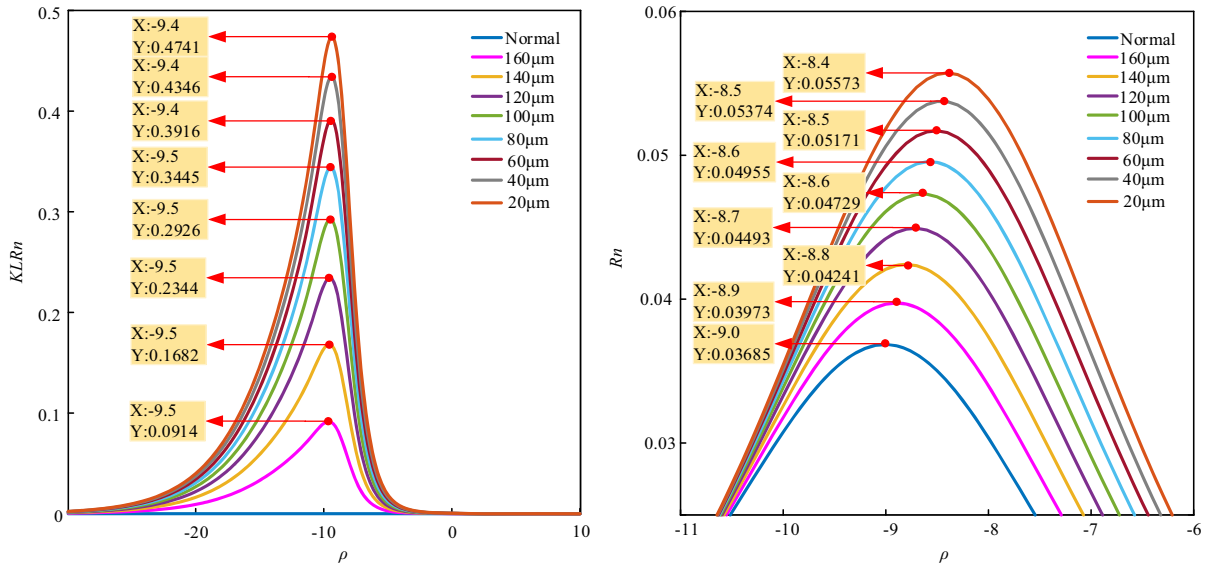

(a) *KLRn* **(b)** *Rn*

Fig. 7 Comparison of *KLRn* and *Rn* curves when friction coefficient is 0.1 (**a-b**)

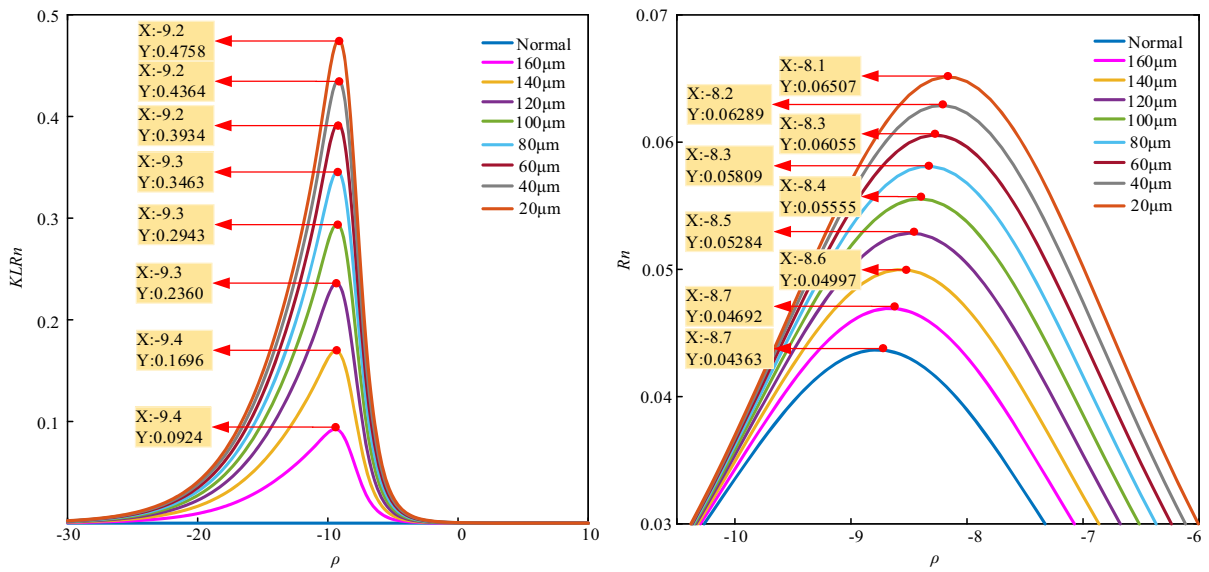

(a) *KLRn* **(b)** *Rn*

Fig. 8 Comparison of *KLRn* and *Rn* curves when friction coefficient is 0.2 (**a-b**)

Step 5: Calculate the value of the proposed index (*KLRm)* through Eq. (25) and then determine the condition of the system qualitatively and quantitatively.

4 Experimental verification

The experimental test bench is illustrated in Fig. 12. The eccentric quality of the disk can be changed by arranging different numbers of bolts in even bolt holes.

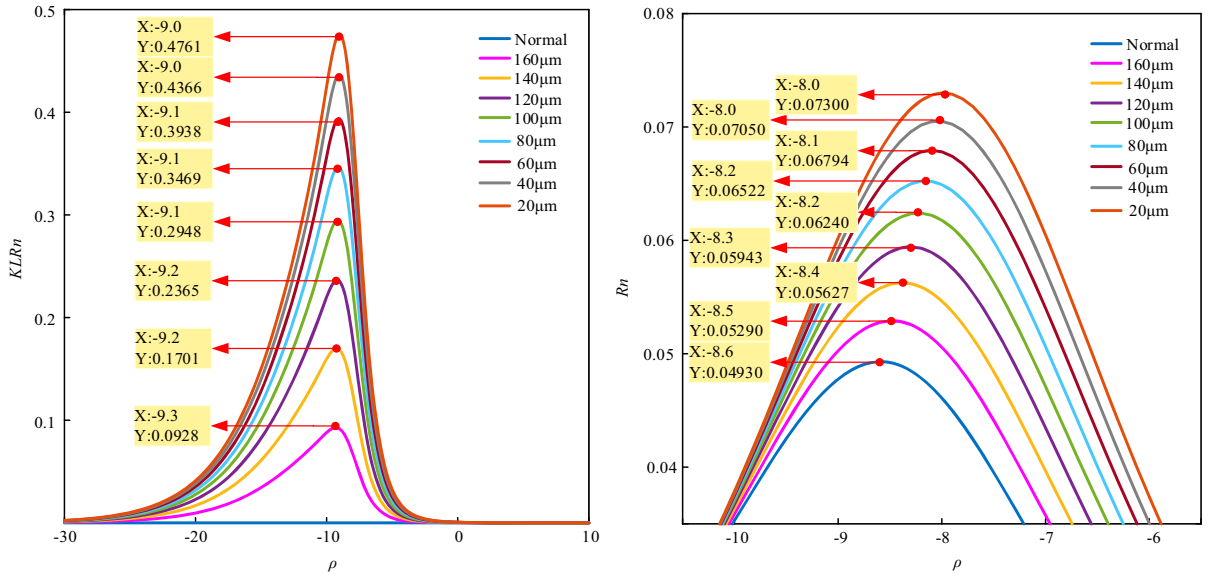

(a) *KLRn* **(b)** *Rn*

Fig. 9 Comparison of *KLRn* and *Rn* curves when friction coefficient is 0.3 (**a-b**)

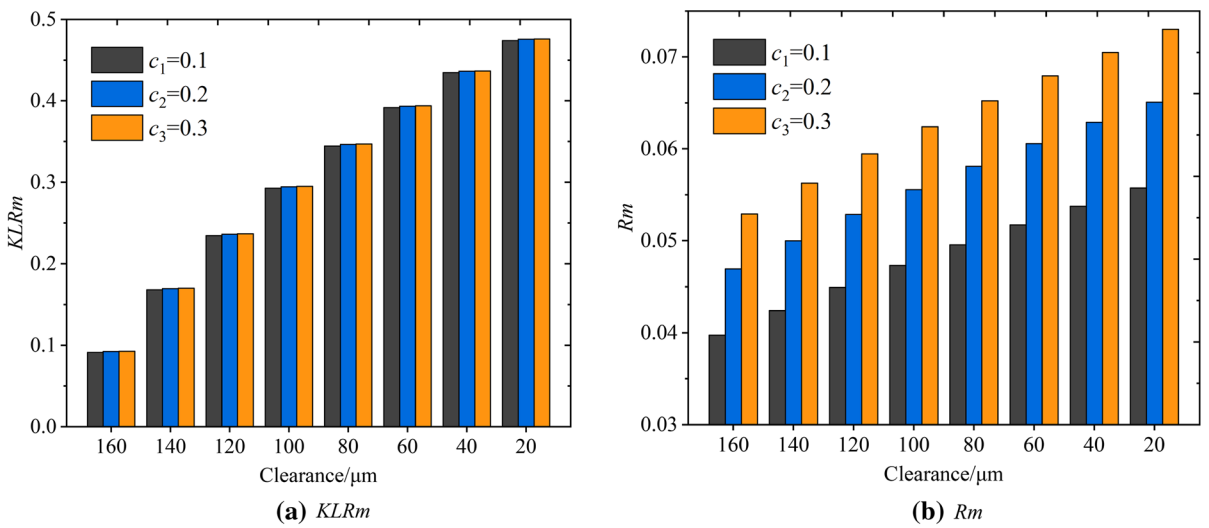

(a) *KLRm* **(b)** *Rm*

Fig. 10 Comparison of *KLRm* and *Rm* under different friction coefficients (**a-b**)

And the rotor system is excited twice with the same frequency but different intensities, namely the same speed but two different unbalances. Different working conditions (normal, weak rub-impact, moderate rub-impact, serious rub-impact, and very serious rub-impact) are implemented by changing the tightening amount of the rub screw. The vibration signals of the rotor system at 1600 rpm under healthy and four different rubbing fault conditions are measured by the eddy current sensor.

Then, each order of the improved NOFRFs weighted contributed rate (*KLRn*1, *KLRn*2, *KLRn*3, *KLRn*4) with the adaptation factor ρ from -40 to 10 with a step of 1.0 under the healthy and the fault conditions are, respectively, calculated. The results are illustrated in Fig. 13.

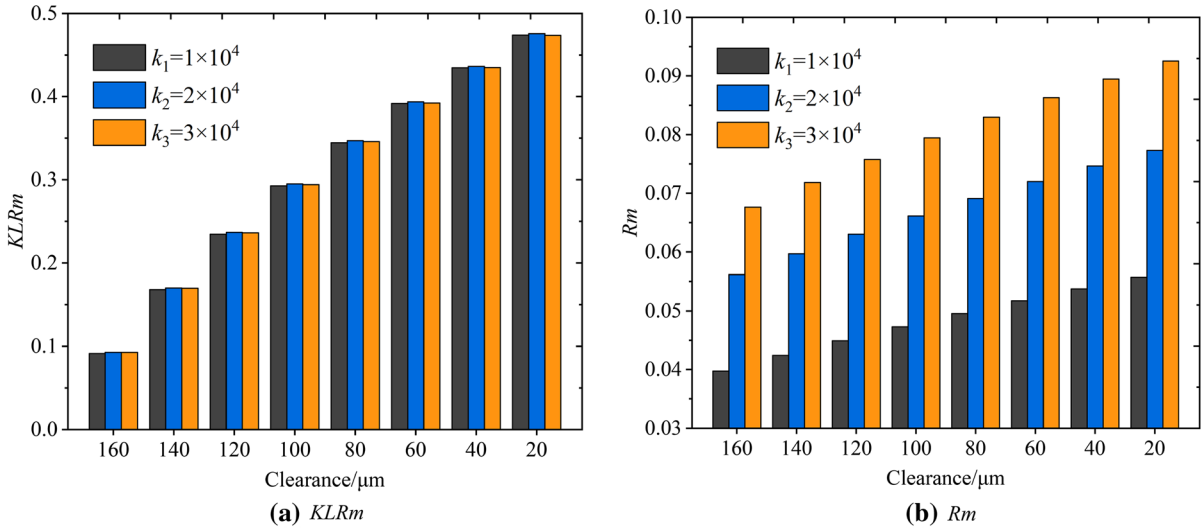

Fig. 11 Comparison of *KLRm* and *Rm* under different rub-impact stiffness (**a-b**)

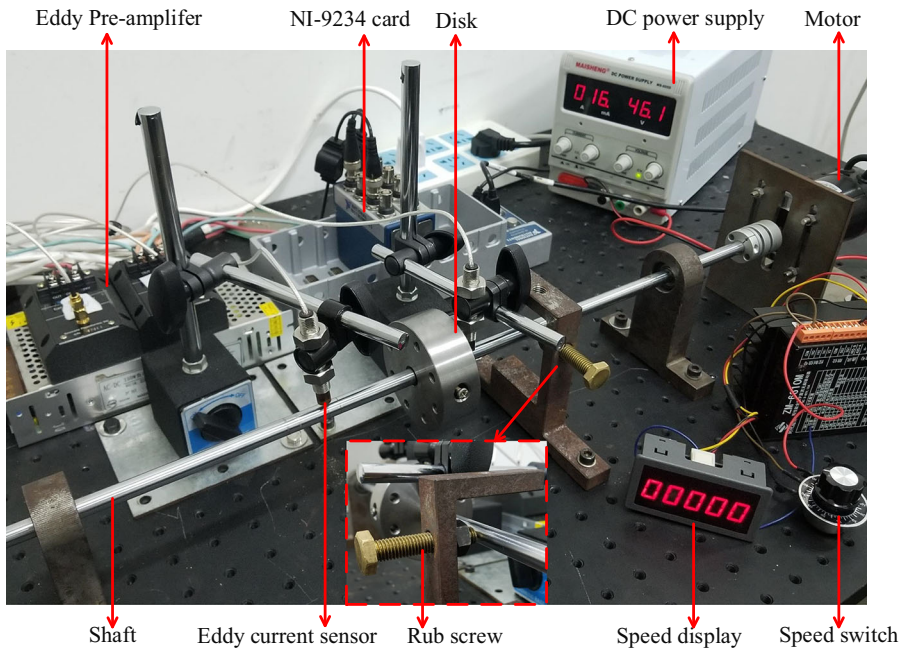

Fig. 12 Experimental test bench of rub-impact rotor system

It can be found from Fig. 13 that the experimental results are similar to the simulation results in Fig. 4. Each order of improved weighted contribution rate, *KLRn*1-*KLRn*4, generally increases first and then decreases. And the peaks of the curves are proportional to the severity of the rubbing fault.

As shown in Fig. 14, it is a comparison of the improved weighted contribution rate, *KLRn*, and the second-order weighted contribution rate, *Rn*, with the change of ρ. The curves of *KLRn* and *Rn* also have a similar trend with that of *KLRn*1-*KLRn*4.

Figure 15 shows a comparison chart of the maximum value of the indexes, *KLRm* and *Rm*. The values of *Rm* increase from 0.16145 to 0.52287 and the values of *KLRm* increase from 0 to 1.13811. Obviously, as the degree of rubbing increases, the change of *KLRm* is significantly greater than that of *Rm*, indicating that the sensitivity of the index *KLRm* to rotor rubbing

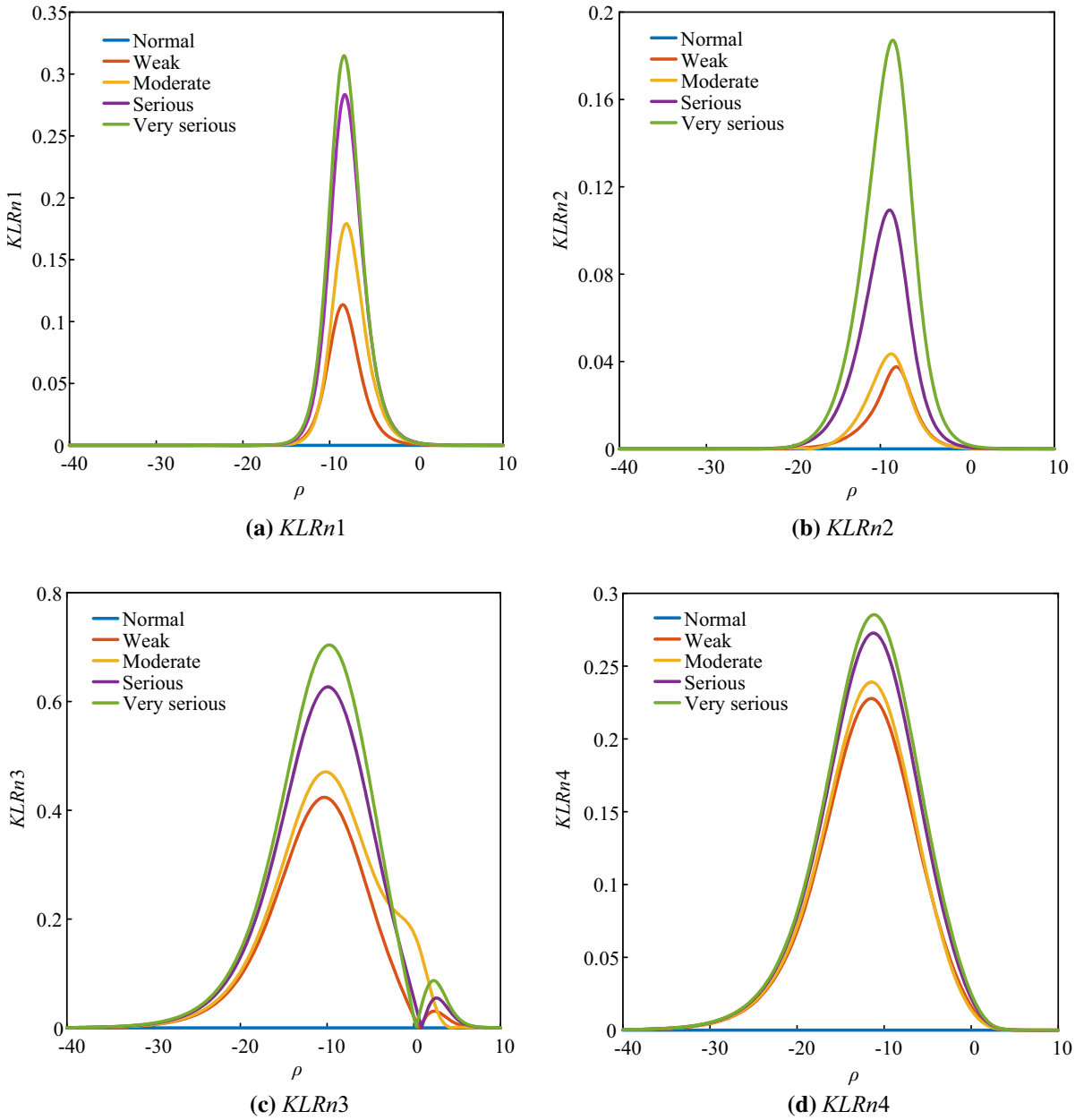

Fig. 13 Each order of *KLRn* at different rub-impact conditions (**a-d**)

faults is greater than *Rm*, which is consistent with the simulation results. Therefore, the improved NOFRFs optimal weighted contribution rate based on KL divergence (*KLRm*) is superior to the second-order optimal weighted contribution rate (*Rm*) in diagnosing the rubbing fault.

5 Conclusion

A method for detecting the rubbing fault of a rotor system was presented in this paper. Based on the method of NOFRFs weighted contribution rate, the KL divergence was introduced and a novel method named improved NOFRFs weighted contribution rate based on KL divergence (NWKL) has been proposed.

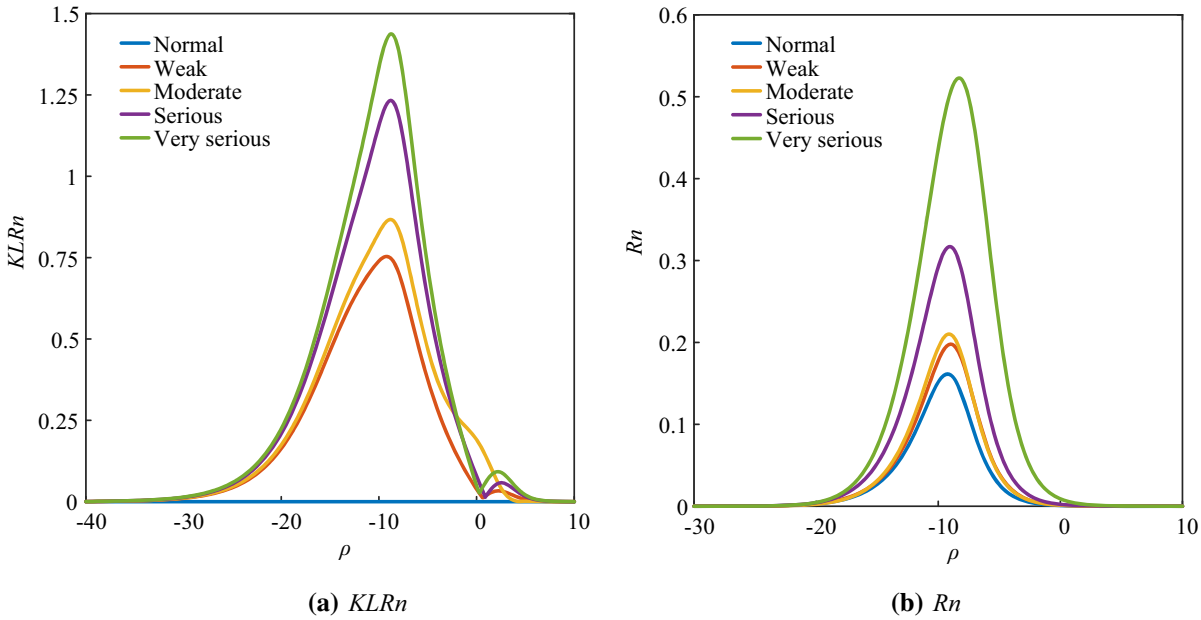

(a) *KLRn* **(b)** *Rn*

Fig. 14 Comparison of *KLRn* and *Rn* at different rub-impact conditions (**a-b**)

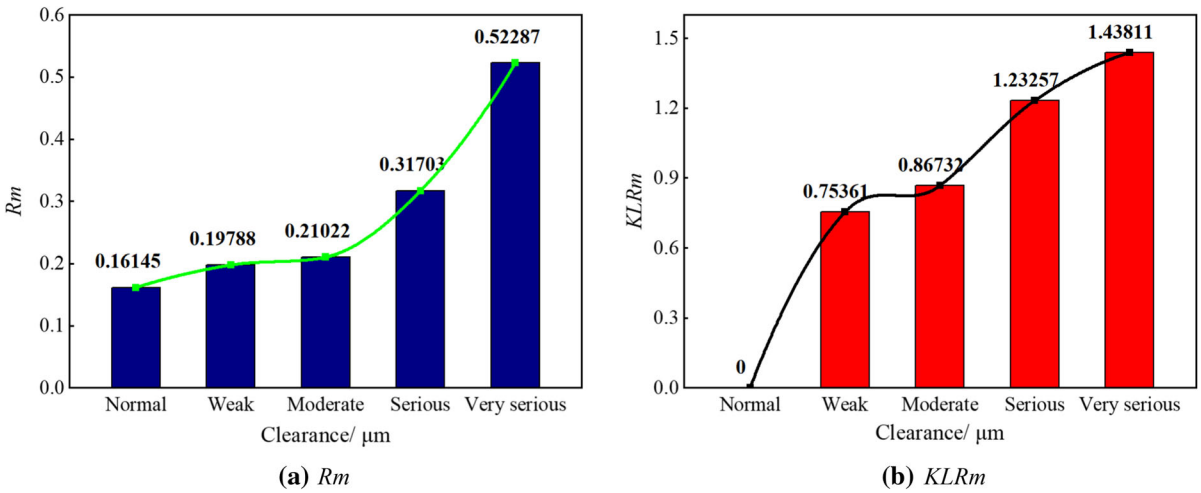

(a) *Rm* **(b)** *KLRm*

Fig. 15 Comparison of *KLRm* and *Rm* at different rub-impact conditions (**a-b**)

A new index was also proposed to diagnose the rub-impact fault severity of the rotor system, which is named the improved NOFRFs optimal weighted contribution rate based on KL divergence (*KLRm*). Furthermore, an evaluation method named feature dynamic stability analysis was proposed to explore the effects of the friction coefficients and rub-impact stiffness on associated indexes. It provides a new research idea for the rubbing fault of the rotor system.

The simulation and experimental results have demonstrated the effectiveness and better superiority of the improved method. Compared with the second-order optimal weighted contribution rate (*Rm*), the newly proposed index (*KLRm*) has higher sensitivity and more robust feature dynamic stability to rub-impact faults of the rotor system. The proposed new approach can comprehensively represent the nonlinear characteristics of a nonlinear system by fusing four orders of NOFRFs weighted contribution rate. It

shows a great application prospect in structural monitoring and fault diagnosis.

Future works will be concerned with the influence of the system nonlinearities on each order of improved NOFRFs weighted contribution rate based on KL divergence. The effectiveness of the proposed index in detecting other fault types of the rotor system needs to be further researched, as well as faults of other nonlinear engineering structures.

Acknowledgements This work is financially supported by the General Program of National Natural Science Foundation of China (Grant No.51875093, Grant No.51105065), the Fundamental Research Funds for the Central Universities from Ministry of Education of China (Grant No. N180304017, Grant No. N2103020) and the National Science Foundation for Postdoctoral Scientists of China (Grant No.2014M551105, 2015T80269).

Declarations

Conflict of interests The authors declare that they have no conflict of interest.

References

1. Chen, L., Qin, Z., Chu, F.: Dynamic characteristics of rub-impact on rotor system with cylindrical shell. Int. J. Mech. Sci. **133**, 51–64 (2017)
2. Zhao, Y., Liu, Y., Xin, X.: Dynamic modelling considering nonlinear factors of coupled spur gear system and its experimental research. IEEE Access. **8**, 84971–84980 (2020)
3. Hong, J., Yu, P., Zhang, D., Ma, Y.: Nonlinear dynamic analysis using the complex nonlinear modes for a rotor system with an additional constraint due to rub-impact. Mech. Syst. Signal Process. **116**, 443–461 (2019)
4. Schoukens, J., Barbe, K., Vanbeylen, L., Pintelon, R.: Nonlinear induced variance of frequency response function measurements. IEEE Trans. Instrum. Meas. **59**(9), 2468–2474 (2010)
5. Chu, F., Lu, W.: Experimental observation of nonlinear vibrations in a rub-impact rotor system. J. Sound Vib. **283**(3), 621–643 (2005)
6. Han, Q., Wang, T., Ding, Z.: Magnetic equivalent modeling of stator currents for localized fault detection of planetary gearboxes coupled to electric motors. IEEE Trans. Ind. Electron. **68**(3), 2575–2586 (2020)
7. Sun, C., Chen, Y., Hou, L.: Steady-state response characteristics of a dual-rotor system induced by rub-impact. Nonlinear Dyn. **86**(1), 1–15 (2016)
8. Swain, A.K., Billings, S.A.: Accurate prediction of non-linear wave forces: Part I (fixed cylinder). Mech. Syst. Signal Process. **12**, 449–485 (1998)
9. Boaghe, O.M., Billings. : Time and frequency domain identification and analysis of a gas turbine engine. Control Eng. Practice. **10**(12), 1347–1356 (2002)
10. Xia, X., Zhou, J.Z., Xiao, J., Xiao, H.: A novel identification method of Volterra series in rotor–bearing system for fault diagnosis. Mech. Syst. Signal Process. **66–67**, 557–567 (2016)
11. Lang, Z.Q., Billings, S.A.: Energy transfer properties of nonlinear systems in the frequency domain. Int. J. Control. **78**, 354–362 (2005)
12. Lang, Z.Q., Billings, S.A., Yue, R.: Output frequency response function of nonlinear volterra systems. Automatica **43**(5), 805–816 (2007)
13. Lang, Z.Q., Park, G., Farrar, C.R., Worden, K.: Transmissibility of non-linear output frequency response functions with application in detection and location of damage in MDOF structural systems. Int. J. Non Linear Mech. **46**(6), 841–853 (2011)
14. Lang, Z.Q., Billings, S.A.: Output frequency characteristics of nonlinear systems. Int. J. Control. **64**(6), 1049–1067 (2015)
15. Peng, Z.K., Lang, Z.Q., Billings, S.A.: Crack detection using nonlinear output frequency response functions. J. Sound Vib. **301**, 777–788 (2007)
16. Peng, Z.K., Lang, Z.Q.: Detecting the position of non-linear component in periodic structures from the system responses to dual sinusoidal excitations. Int. J. Non Linear Mech. **42**, 1074–1083 (2007)
17. Bayma, R.S., Zhu, Y., Lang, Z.Q.: The analysis of nonlinear systems in the frequency domain using nonlinear output frequency response functions. Automatica **94**, 452–457 (2018)
18. Yao, H., Han, Q., Li, L., et al.: Detection of rubbing location in rotor system by super–harmonic responses. J. Mech. Sci. Technol. **26**(8), 2431–2437 (2012)
19. Cao, J., Chen, L., Zhang, J., Cao, W.: Fault diagnosis of complex system based on nonlinear frequency spectrum fusion. Measurement **46**(1), 125–131 (2013)
20. Peng, Z.K., Lang, Z.Q., Wolters, C., Billings, S.A., Worden, K.: Feasibility study of structural damage detection using NARMAX modelling and nonlinear output frequency response function based analysis. Mech. Syst. Signal Process. **25**, 1045–1061 (2011)
21. Huang, H.L., Mao, H.Y., Mao, H.L.: Study of cumulative fatigue damage detection for used parts with nonlinear output frequency response functions based on NARMAX modelling. J. Sound Vib. **411**, 75–87 (2017)
22. Liu, Y., Zhao, Y., Lang, Z.Q.: Weighted contribution rate of nonlinear output frequency response functions and its application to rotor system fault diagnosis. J. Sound Vib. **460**, 114882 (2019)
23. Liu, Y., Zhao, Y.L., Li, J.T.: Application of weighted contribution rate of nonlinear output frequency response functions to rotor rub-impact. Mech. Syst. Signal Process. **136**, 106518 (2020)
24. Liu, Y., Li, J.T., Feng, K.P.: A novel fault diagnosis method for rotor rub-impact based on nonlinear output frequency response functions and stochastic resonance. J. Sound Vib. **481**, 115421 (2020)

25. Mao, H., Tang, W., Zhu, W., Yang, G., Si, B.: Feasibility study on wheelset fatigue damage with nofrfs-kl divergence detection method in simo. J. Sound Vib. **483**, 115447 (2020)
26. Hua, C., Rao, Z., Ta, N., Zhu, Z.: Nonlinear dynamics of rub-impact on a rotor-rubber bearing system with the stribeck friction model. J. Mech. Sci. Technol. **29**(8), 3109–3119 (2015)